A critical period for auditory thalamocortical connectivity

Tania Rinaldi Barkat[1], **Daniel B. Polley**[2], and **Takao K. Hensch**[1]

[1]Center for Brain Science, Dept Molecular & Cellular Biology, Harvard University, 52 Oxford Street, Cambridge, MA 02138 USA

[2]Eaton-Peabody Laboratory, Massachusetts Eye and Ear Infirmary, Dept of Otology and Laryngology, Harvard Medical School, Boston MA 02114 USA

Abstract

Neural circuits are shaped by experience during periods of heightened brain plasticity in early postnatal life. Exposure to acoustic features produces age-dependent changes through largely unresolved cellular mechanisms and sites of origin. Here, we isolated the refinement of auditory thalamocortical connectivity by *in vivo* recordings and day-by-day voltage-sensitive dye imaging (VSDI) in an acute brain slice preparation. Passive tone-rearing modified response strength and topography within mouse primary auditory cortex (A1) during a brief, three-day window but failed to alter tonotopic maps in the thalamus. Gene-targeted deletion of a forebrain-specific, cell-adhesion molecule (*Icam5*) accelerated plasticity in this critical period. Consistent with its normal role to slow spinogenesis, loss of *Icam5* induced precocious stubby spine maturation on pyramidal cell dendrites in neocortical layer 4 (L4), identifying a primary locus of change. The evolving postnatal connectivity between thalamus and cortex in the days following hearing onset may thus determine a critical period for auditory processing.

Neural circuits are shaped by experience during periods of heightened brain plasticity in early life[1,2]. Children raised in an English-speaking environment will easily distinguish between the phonemes /la/ and /ra/, whereas those growing up in Japan find it increasingly difficult[3]. Passive exposure of young rodents to a variety of sound features reveals a cascading series of developmental windows which open and close shortly after hearing onset to define the persistent and specific influences of early experience on the functional organization of auditory cortex[4–6]. The underlying sites of plasticity along the auditory pathway, as well as potential mechanisms engaged during such critical periods remain to be elucidated.

Motivated by the well-known binocular interactions shaped by experience in developing visual cortex[7–9], we first applied *in vivo* neurophysiological recordings to determine whether mouse A1 also exhibits a critical period for tonotopic map plasticity induced through passive tone exposure, and whether such plasticity was also present in the auditory thalamus (ventral medial geniculate body, MGBv). We then isolated the connection between MGBv and A1[10] in an acute brain slice preparation[11] and applied VSDI techniques *in vitro*. We mapped A1 responses to electrical stimulation of discrete sites in MGBv across early postnatal days (P8 to P20), following tone-rearing or gene manipulation. Our results reveal a critical period for acoustically-driven topographic plasticity at thalamocortical connections in mouse A1.

METHODS

In vivo electrophysiology

All experimental procedures were carried out according to Harvard and Vanderbilt University animal care and use guidelines. A1 and MGBv recordings were made from the left hemisphere at P28–P40. Mice were brought to a surgical plane of anesthesia using a combination of pentobarbital sodium (50 mg/kg followed by 10–15 mg/kg supplements as needed) and chlorprothixene (0.2 mg). Multiunit responses were recorded from the middle cortical layers of A1 (420–440 μm from pial surface) with epoxylite-coated tungsten microelectrodes (2.0 MΩ at 1 kHz, FHC) and from MGBv with 16-channel silicon probes (177 μm^2 contact area, 50 μm inter-contact separation, Neuronexus Technologies). Frequency response areas were measured with pseudo-randomly presented tone pips of variable frequency (5.5 to 45.3 kHz in 0.1 octave increments, 20 ms duration, 5 ms raised cosine onset/offset ramps, 0.6 sec intertrial interval, 1 presentation per unique tone/level combination) and level (0–60 dB SPL in 5 dB increments) delivered from a free field electrostatic speaker placed 12 cm from the contralateral ear.

Best frequency was defined for each recording site as the tone frequency that evoked the greatest number of spikes. A1 was readily identified by a clear caudal-to-rostral low-to-high best frequency gradient and was bounded by sharp best frequency reversals or unresponsive sites as described previously[13,44]. A topographic analysis of best frequencies was achieved by dividing the map into equal thirds along the caudal-to-rostral extent and separately analyzing best frequencies in each sector (Figs.1f, g and 2f). No significant differences were found in the spatial sampling density within each sector of the map, justifying comparisons of overall best frequency distributions between groups (P=0.56 for P11–P15 versus no exposure and P=0.29 for P16–P20 versus no exposure, Chi-square test).

For MGBv, a multi-channel silicon probe was inserted under stereotaxic guidance at the same dorsoventral angle used for the brain slice preparation to effectively isolate it from other thalamic sub-divisions. This was confirmed by carefully noting a reversal in the best frequency gradient marking the medial edge of MGBv, and by *post mortem* reconstruction of electrode tracks and lesion sites according to methods described in a recent study[13].

Acute auditory thalamocortical slice preparation

C57BL/6J (Jackson Lab, Bar Harbor, ME) or *Icam5*$^{-/-}$ (c/o M Mishina, Univ Tokyo) mice (P8–P20) were rapidly decapitated without anesthesia and placed in ice-cold ACSF. Slices were sectioned on a vibratome (Microm HM 650V, Thermo scientific, Walldorf, Germany) according to the method of Cruikshank et al[11]. Briefly, 600 μm thick horizontal slices with the lateral end raised 15°, were cut in ice-cold ACSF and incubated at 35°C for at least 15 minutes, before returning to room temperature (20–22°C). One left hemisphere slice was used per animal. The ACSF contained (in mM) 125 NaCl, 25 glucose, 25 NaHCO$_3$, 2.5 KCl, 2 CaCl$_2$, 1.25 NaH$_2$PO$_4$, 1 MgCl$_2$ (315–328 mOsm).

Voltage-sensitive dye imaging

Voltage-sensitive dye Di-4-ANEPPS (Invitrogen cat#D-1199) dissolved at 0.01 mg/ml in dimethylsulfoxide stock solution was diluted (0.6 μl/ml) in ACSF, for a final solution of 5 μg/l Di-4-ANEPPS. Slices were incubated for at least 90 min before transfer to an ACSF (room temperature) recording chamber. Slices were imaged using an Olympus MVX10 microscope with 1×0.25 numerical aperture (NA) objective. Excitation light from a shuttered 150 W halogen lamp (MHF-G150LR, Moritex Corporation, Japan) was band-pass filtered (515/35 nm) and reflected toward the sample by a 570 nm dichroic mirror. Emitted fluorescence, reflecting a change in potential across neuronal membranes[45,46] (Supplementary Fig.3), was long-pass filtered (590 nm) and imaged using a MiCam Ultima CMOS based camera (SciMedia, Tokyo, Japan). Fluorescent changes (1 ms frame rate for 512 ms periods) were averaged across 10 trials and integrated across different regions of interest containing 5×5 pixels covering 125×125 μm by spatial averaging and across different trials using MiCam Ultima analysis software.

Individual time-course traces were subsequently exported to Igor Pro (WaveMetrics, Portland, OR) to combine data for a number of slices. Fluorescence change was normalized to resting fluorescence (ΔF/F$_0$). Stimulation was controlled by a programmable pulse generator (MiCam Ultima software, SciMedia, Tokyo, Japan) linked to a constant current stimulus isolation unit (Iso-Flex, A.M.P.I., Jerusalem, Israel). Discrete sites in the MGBv were activated with an ACSF-filled patch pipette (0.5 mA, 1 ms pulse) at 100 ms after recording onset.

Response amplitude was defined as maximum fluorescence change (ΔF/F) per trial at a given region of interest. Peak amplitude was defined as maximum response amplitude across all L4 locations. Variations in daily preparation were normalized by slice: all signals were divided by the maximum change in fluorescence measured in a set of experiments (Norm. ΔF/F = (ΔF/F)/max(ΔF/F)). Response latency was defined as the time elapsed from stimulus pulse to half-maximal signal amplitude. As VSDI reports relative changes in fluorescence as a function of membrane potential fluctuation[45], the absolute changes in fluorescence might reflect a number of technical as well as biological considerations (such as differential staining / transparency). Therefore, our VSDI results are presented as normalized signals for comparison across ages and conditions.

Strongest signals as a function of MGBv stimulus site were taken from regions of interest along the rostro-caudal axis of A1 at a constant distance from an anatomical landmark chosen as reference (most rostral point X of hippocampus in Supplementary Fig.5) and at constant depth from the pia, corresponding to upper L4 based on Nissl stains (Fig.5a), covering a total distance of 2250 μm. The stimulating electrode was positioned on the rostral MGBv at six discrete positions spaced at 100 μm intervals along the medio-lateral axis (Supplementary Fig.5, landmark 4 for stimulus site 1)[13].

For columnar analysis, regions of interest where the signal in upper L4 was strongest, were chosen along the medio-lateral A1 axis orthogonal to the pia, for a total distance of 1000 μm. The stimulating electrode was placed in the most rostral part of the MGBv where the stimulus could evoke the strongest response in A1 (Supplementary Fig.5, landmark 5). To assess any polysynaptic contribution, a modified ACSF with high divalent cation (X^{++}) content was used[11] (in mM): 115 NaCl, 25 glucose, 25 $NaHCO_3$, 2.5 KCl, 7.2 $CaCl_2$, 4.2 $MgCl_2$ (315–325 mOsm). To confirm the synaptic nature of the response, 40 μM D-APV and 10 μM CNQX were added to the ACSF at the end of most experiments (Supplementary Fig. 2b).

Sound exposure

Subsets of mouse pups and mothers were placed in a sound-attenuating chamber (IAC, Bronx, NY) and exposed to 7 or 20 kHz tones (100 ms pulses at 5 Hz[47,48] for one second followed by two seconds of silence, 78 or 73 dB SPL, respectively). A 7 kHz frequency was chosen as the middle of the sound spectrogram for mouse pup wriggling calls[49], and therefore ethological for mice of this age. Mice were otherwise reared under standard conditions (12:12 h light:dark cycle, access to water and food *ab libitum*) and moved about freely in their cage. Audible (7 kHz) tones were generated by Audacity software (http://audacity.sourceforge.net/) and amplified by speakers placed in two corners of the chamber. High-frequency (20 kHz) tones were generated by Adobe Audition software and amplified by an electrostatic speaker driver (ED1) and electrostatic speaker (ES1, Tucker Davis Technologies, Alachua, FL) placed on top of the mouse cage.

Subsets of mice were exposed to 7 kHz tones from P8 until recording (removed less than 30 minutes prior to decapitation) around P20 (P19–P21). Other subsets were exposed for shorter time windows: from P8 to P11, from P12 to P15, from P16 to P19, or from P12 to P13, P13 to P14, P14 to P15, P12 to P14, P13 to P15; then returned to standard housing conditions until decapitation around P20 for VSDI.

DiI labelling

C57BL/6J mice at P13 or P16 (Jackson Lab, Bar Harbor ME) or *Icam5*−/− mice at P13 were anesthetized with nembutal (50 mg/kg) and perfused transcardially with 0.9% saline and 4% para-formaldehyde in PBS. Brains were trimmed and thalamocortical slices cut (200 μm thick) for 'DiOlistics' labeling with lipophilic dye (DiI, Molecular Probes) coated on tungsten particles (0.7 μm diameter, Bio-Rad, UK)[50]. Density of labelling was controlled by gas pressure (200 psi helium) and no other filters. Randomly labelled pyramidal neurons situated in upper L4 of A1 were selected by confocal microscopy (40× air objective, 3×

zoom; FluoView1000, Olympus, Tokyo, Japan). Images at 0.25 μm steps were acquired and stacked for 3D reconstruction using FluoView software. Neurites were reconstructed within a radius of 100 μm from the soma using Neurolucida (MicroBrightField, Williston, VT). All protrusions along apical and basal dendrites were counted. Those with distinct heads and head diameter larger than neck diameter were classified as mushroom spines, while dendritic protrusions without distinct heads were classified as stubby spines[23]. Spines that were thinner than 0.3 μm and longer than 2 μm, defined as filopodia or thin spines, were not counted.

Immunohistochemistry

Standard protocols were used to label thalamocortical slices. Briefly, slices (600 and 100 μm thick for Nissl and ICAM5staining, respectively) kept in paraformaldehyde (4%) overnight at room temperature, then washed in PBS, solubilised and blocked in triton X-100 (0.8%), BSA (20%) in PBS (4°C overnight) were incubated for Nissl stain with NeuroTrace 435/455 (Molecular Probes, Eugene, OR) or rabbit polyclonal anti-*Icam5* (c/o Y Yoshihara, RIKEN BSI)[21] in BSA (5%) in PBS (4°C overnight) followed by a fluorescent secondary antibody.

In vitro patch clamp recording

Slice preparation and stimulation protocols were same as for the VSDI experiments. Whole-cell recordings of upper L4 pyramidal neurons were amplified using Axopatch 200B amplifiers (Axon Instruments, Molecular Devices, Union City, CA). Voltages (in current-clamp mode) were recorded with pipettes containing (in mM) 120 potassium gluconate, 10 KCl, 4 ATP-MG, 10 phosphocreatine, 0.3 GTP, 10 HEPES, and 0.2% biocytin (pH 7.3, 290 mOsm). For each slice, up to three cells per stimulus site (1, 3 and 5) and L4 location (8, 10 and 13, respectively) were patched, and the cell with the strongest response (average of 30 traces, clamped at −70 mV) was used for the analysis.

Statistical analyses

Results are reported as mean ± s.e.m and compared across groups using a two-tailed, unpaired Student's t-test with statistical significance at $P<0.05$ if n was bigger than 10, where n represents the number of animals, or neurons for Figs.1, 2, and 7, per experiment. For small data samples (n<10), or where the assumption of a Gaussian distribution could not be verified, results were reported as median ± s.e.m, and the nonparametric two-tailed Mann-Whitney U or Wilcoxon rank sum test was used (Figs. 4e, 5b, 6, 7 and Supplementary Fig.3b) with statistical significance at $P<0.05$. Input strength distributions (Fig.4a) and gradient of peak locations (Fig.4c) were compared with two-way ANOVA tests. Best frequency distributions (Figs.1e and 2e) were compared with two-sample Kolmogorov-Smirnov tests.

RESULTS

Tone exposure modifies tonotopic maps in A1 but not MGBv

The auditory system is tonotopically organized[10], such that tones of similar frequency activate neighboring neurons at each station along the pathway. As rats show experience-dependent tonotopic map reorganization following passive tone exposure during the second

postnatal week[2, 12], we first used high-density *in vivo* mapping to delineate A1 tonotopy in young adult mice[13] that were reared either in typical acoustic environments (Fig.1a) or in the presence of pulsed 7 kHz tone pips from P11–P15 (Fig.1b) or P16–P20 (Fig.1c). Comparison of representative tonal receptive fields drawn from caudal, intermediate and rostral map locations (Fig.1d), demonstrates that tone rearing from P11–P15, but not P16–P20, was sufficient to shift A1 best frequencies toward the 7 kHz exposure frequency (Fig. 1e; P11–P15, n=5 mice/93 sites versus no exposure, n=5 mice/93 sites, *P*=0.003; P16–P20, 4 mice/64 sites versus no exposure, *P*=1.0, Kolmogorov-Smirnov test). Upon closer inspection, expansion of best frequency representations near the exposure frequency was attributable to topographically-specific reallocation of best frequencies in caudal and intermediate regions of the tonotopic map proximal to where 7 kHz is normally represented, rather than a shift in more rostral map areas that retain normal tuning to higher frequencies (Fig.1f, g; *P*=0.009, 0.04, and 0.14 for P11–P15 versus. no exposure at caudal, mid and rostral locations, respectively, t-test).

To determine whether remapping in A1 could be explained by a shifted frequency representation within the principal subcortical input source, we also examined best frequency distributions in the MGBv. A multichannel silicon probe was inserted at an angle that matched the plane of section used in subsequent thalamocortical slice experiments[11] (Fig.2a). This approach allowed us to sample the low-to-high, lateral-to-medial best frequency gradient within MGBv *in vivo* (Fig.2b) with a comparable multiunit signal-to-noise ratio as our A1 recordings (Fig.2c), while excluding recordings from auditory areas medial to MGBv (Fig.2d and Methods). Although 7 kHz rearing from P11–P15 induced a significant shift in A1 maps (Fig.1), we found no evidence for shifts in overall best frequency distributions within MGBv (Fig.2e; P11–P15, n=5 mice/151 sites versus no exposure, n=4 mice/101 sites; *P*=0.99, Kolmogorov-Smirnov test) or differences in mean best frequency at lateral (50 μm into MGBv), more medial (200 μm into MGBv) or across all recording sites (Fig.2f, *P*=0.44, 0.18 and 0.91 at lateral, medial and overall locations, respectively, t-test). In contrast, other auditory receptive field changes, such as specific reductions in best frequency tuning bandwidth, were found in both MGBv recordings (P11–P15) and throughout A1 (P11–P20) (Supplementary Fig.1).

A developmental time window for A1 response maturation

In the rodent MGBv, the gradient of preferred sound from low (lateral) to high (medial) frequency allows us to mimic tones of varying frequency across the latero-medial axis *in vitro*[13–15]. We stimulated the MGBv at six different loci along this dimension in brain slices preserving the thalamocortical connection to A1 (Fig.3a, colored arrows)[11] and used VSDI to measure cortical response (Supplementary Fig.2). Discrete current pulses to MGBv yielded topographically distinct, maximal responses across upper L4 of A1 to derive a map of peak amplitudes as function of stimulus site (Fig.3a, L4 loci)[13].

In young animals (P8–P12), responses to lateral MGBv loci were significantly weaker than to medial stimuli (Fig.3b, peak F/F at locus 1 =0.30±0.06 versus locus 6 =0.82±0.05, n=13 each; *P*<0.00001, t-test). This inhomogeneous distribution of peak amplitudes gradually disappeared with brain maturation. After P15, peak cortical responses were similar across

stimulus sites (Fig.3b). Interestingly, the adjustment of thalamocortical response strength occurred within three days between P12 and P15, coinciding with the emergence of adult-like A1 neural response thresholds for airborne sound transmission[6,16]. We validated these network modifications over development at synaptic resolution by direct patch-clamp recording from upper L4 pyramidal neurons in mice younger than P12 compared to those older than P15 (Supplementary Fig.3).

Interestingly, the mapping of peak response within L4 as a function of MGBv stimulus site did not change during the same developmental period studied (P8–P20). As indicated by the linear relation of peak   F/F position in L4 to MGBv input ('topographic slope'; Fig.3c), an orderly spatial layout of this pathway was already present prior to hearing onset[16] even as connection strengths were still maturing across the map (Fig.3b).

A critical period for thalamocortical connectivity

Normal acoustic experience therefore does not modify the intrinsic organization of thalamocortical input present at hearing onset. In contrast, if the mouse were exposed early to an abnormal acoustic environment, the topography was dramatically altered. Maximal A1 responses along the rostro-caudal L4 axis in P16–P20 mice were concentrated near a single, middle MGBv input (dashed) after continuous exposure to 7 kHz tone pips from P8 (Fig.4a, b). Although the strength of cortical responses retained homogeneity across stimulus sites, a clear flattening of topographic slope was evident in L4 (Fig.4c). This direct functional rearrangement of thalamocortical response was confirmed by comparing distributions of input strength for two independent stimulus sites (1 and 6) (control: P=0.003, exposed: P=0.181, ANOVA test) as well as the gradient of peak locations (P=0.029, ANOVA test) in control and exposed mice.

By exposing mice to 7 kHz tones for shorter, three-day intervals (P8–P11; P12–P15; P16–P19; Fig. 4d), significant topographic reorganization was found only when mice were exposed from P12–P15 (Fig.4e; topographic slope at P20: no exposure =1.42±0.37, n=9; versus P12–P15 exposure =0.07±0.13, n=8; P=0.026, Mann-Whitney U test). This identified a critical period for mouse auditory thalamocortical topography that coincides with the normal time window during which this connection is maturing (Fig.3b) and for tonotopic map changes *in vivo* (Fig.1). Topographic remapping was not restricted to 7 kHz, as passive tone exposure to 20 kHz (from P12–P15) produced a similar topographic reorganization at a correspondingly more rostral A1 locus (Supplementary Fig.4).

Laminar shift of connectivity during the critical period

We further examined the emergence of A1 responses along a cortical column during postnatal development. As expected, the maximum response amplitude to MGBv stimulation was located in upper L4 at 325±75 μm from the pial surface for all ages studied (Fig.5a). Although each thalamocortical preparation is unique, the variability in geometry and size of various anatomical hallmarks relative to a reference point (the rostral tip of the hippocampus, X in Supplementary Fig.5) was insignificant across the developmental period studied (Supplementary Fig.5). Notably, changes in total cortical thickness across these ages were negligible (<10 μm/bin) with respect to the individual bin sizes. However, the location

of shortest response latency shifted significantly upward along the column over the course of the critical period for plasticity defined above (Fig.5a; minimum latency site: P8–P11 =900±75 μm, grey arrow; P16–P20 =325±75 μm, black arrow). This was true across the entire rostro-caudal extent of A1 (Supplementary Fig.6).

Moreover, when polysynaptic activity was weakened in a modified (high divalent cation, X^{++}) artificial cerebrospinal fluid (ACSF)[11], the strong signal observed in upper L4 was significantly reduced at P8–P12 but not for older animals (Fig.5b; (F/F_{normal}− $F/F_{highX++}$)/ F/F_{normal}: P8–P12 =0.40±0.13, n=6 versus P13–P15 =0.01±0.06, n=8; or P16–P20 =0.01±0.05, n=4; P=0.020 and 0.038, respectively, Mann-Whitney U test). Tone exposure did not affect this upward translocation of direct thalamocortical input to L4, as verified by little reduction of peak signal in high divalent cation ACSF for mice passively exposed to 7 kHz (P16–P20 =0.11±0.19, n=4). These results indicate that thalamic inputs initially target their synapses to deeper regions, most probably the subplate (a transient zone in the developing neocortex)[17–19] prior to invading L4 during the critical period.

Forebrain-selective gene deletion accelerates plasticity

To establish a thalamocortical mechanism for this critical period plasticity, we analyzed a mouse model carrying a forebrain-specific gene deletion. *Icam5* is an intercellular adhesion molecule expressed exclusively in the telencephalon[20] and is sorted into dendrites of pyramidal cells to slow spine maturation[21] (Fig.6a). Notably, *Icam5* is not expressed in the MGBv or other subcortical structures in wild-type animals, and is absent throughout the brain of knockout (*Icam5*^{−/−}) mice (Fig.6b).

Consistent with a role for *Icam5* as a negative regulator of spine maturation, peak A1 response strength in upper L4 of *Icam5*^{−/−} mice matured rapidly to a homogeneous distribution in just one day from P12 to P13 (Fig.6c), unlike the typical three days for wild-type animals (Fig. 3b). By P13, *Icam5*^{−/−} mice already exhibited a fully mature amplitude distribution comparable to P16 wild-type mice (Supplementary Fig.7a). Moreover, the upward shift of columnar response latencies occurred faster in *Icam5*^{−/−} mice and was also mature by P13 (Supplementary Fig.7b). These animals exhibit stronger long-term potentiation and hippocampal learning behavior[20], suggesting a similar mechanism may be at work for thalamocortical synapses in L4.

As the period of normal circuit maturation corresponds to the critical period for topographic changes in wild-type mice (Figs.3b and 4e), we tested whether plasticity would also be accelerated in *Icam5*^{−/−} mice. Topography was identical to wild-type when *Icam5*^{−/−} mice were raised in normal acoustic environments (Fig.6d). However, exposing animals to 7 kHz tones for just one day (P12–P13) significantly altered topography at P16–P20 in *Icam5*^{−/−}, but not in wild-type mice (Fig.6d; topographic slope: wild-type =0.86±0.20, n=9 versus *Icam5*^{−/−} =0.23±0.10, n=7; P=0.014, Mann-Whitney U test). Even two days of exposure were insufficient to yield topographic changes in wild-type mice (P12–P14 or P13–P15, Supplementary Fig.7c).

Exposing *Icam5*^{−/−} mice between P13–P14 also altered topography, but to a lesser extent than at P12–P13 (Fig.6d; topographic slope: *Icam5*^{−/−} not exposed =0.97±0.03, n=9 versus

Icam5$^{-/-}$ exposed between P13–P14 =0.25±0.22, n=9; *P*=0.048, Mann-Whitney U test). Even later exposure between P14–P15 (Fig.6d) or before the typical critical period (P8–P11, Supplementary Fig.7c) did not cause any significant change in the topographic organization of *Icam5*$^{-/-}$ mice. Thus, the critical period itself is not shifted earlier in time but shortened in duration in the absence of forebrain-specific *Icam5*. These findings underscore indications from wild-type mice that the tonotopic critical period directly reflects a transition in the maturational state of thalamocortical connections[22].

Stubby spine density increases through the critical period

Given the role of *Icam5* to slow filopodia-to-spine transitions[21], we examined whether enhanced spinogenesis might contribute to the accelerated critical period plasticity in *Icam5*$^{-/-}$ mice. Notably, dendritic spines in L4 within a 100 μm radius around cortical pyramidal cell somata are reported to receive direct thalamocortical input (Fig.7a)[23]. Spines in this region were significantly more dense at P13 in *Icam5*$^{-/-}$ mice compared to wild-type (Fig.7b; spine density: wild-type =0.32±0.02 μm^{-1}, n=6 neurons /1777 spines versus *Icam5*$^{-/-}$ =0.42±0.02 μm^{-1}, n=7 neurons/2567 spines; *P*=0.0012, Mann-Whitney U test).

Interestingly, this increase was significant only for stubby spines (wild-type density =0.24±0.02 μm^{-1}, n=1277 spines versus *Icam5*$^{-/-}$ density =0.33±0.02 μm^{-1}, n=1992 spines; *P*=0.001, Mann-Whitney U test), which are preferentially targeted by MGBv thalamic afferents[23]. Likewise in wild-type mice, a later increase in stubby spine density was eventually observed by P16, marking the end of their typical critical period for tonotopic plasticity (Fig.7c; 0.44±0.03 μm^{-1}, n=7 neurons /2534 spines). Thus, dendritic spine maturation on thalamo-recipient cortical neurons is a likely locus defining the temporal window for topographic map plasticity in A1.

DISCUSSION

We have identified with ever-finer resolution a developmental plasticity occurring at thalamocortical connections related to tonotopy in A1. Accelerated refinement in the absence of a forebrain-specific molecule, *Icam5*, and the stability of MGBv *in vivo* upon tone exposure, both support the view that this critical period reflects dendritic spine maturation on L4 neurons in A1.

Previously, tonotopy has mainly been assessed by micro-electrode recording of spiking activity in response to a given tone[5, 12]. The resultant best frequency maps exhibit relatively precise point-to-point correlation between tone frequency and its preferred site in the cortical map (Figs.1 and 2). In contrast, VSDI in a slice preparation reveals that stimulation of a point in MGBv recruits activity from a broad swath of the A1 map that reflects primarily sub-threshold, monosynaptic activation rather than polysynaptic intra-cortical excitation (Fig. 5b). The same discrepancy is observed in rodent barrel cortex, where *in vivo* microelectrode recordings suggest a highly focused mapping between a single whisker and its corresponding barrel[24], while *in vivo* VSDI or intrinsic signal imaging demonstrate that stimulation of a single whisker can evoke significant activity across a much broader area of the barrel cortex[25–27].

Both the somatosensory imaging studies as well as our own data in A1[13] confirm that the spatial peak of the sub-threshold activity profile closely corresponds to the map of preferred stimuli obtained with microelectrode mapping. This reinforces our use of VSDI peak and its topographic slope to track developmental and experiential changes in thalamocortical function and to relate these changes to observations made through conventional mapping of best frequencies (Figs.1 and 2). At the single-cell level, direct whole-cell recordings of synaptic strength across ages further corroborated the use of VSDI peak measurements (Supplementary Fig.3). Our imaging approach therefore provides the appropriate spatial resolution to bridge the gap between *in vivo* network and *in vitro* cellular observations of plasticity mechanism in the developing auditory system.

With its sub-millisecond time resolution, VSDI further reveals the sequence of activation within a given zone, for example across the topographic extent of A1[13] or along a cortical column. This technique can therefore resolve fast monosynaptic connections from the thalamus and slower, polysynaptic, intracortical inputs. During maturation[17,19], deeper regions comprised of the subplate, a transient neocortical structure present in several cortical areas early in development, are largely replaced by the cortical plate, in particular L6. Subplate neurons send strong excitatory projections up to L4, which may regulate activity-dependent processes that catalyze the maturation and plasticity of the developing cortex[19].

At the cellular level, the mechanism of plasticity is related to stubby spine maturation proximal to the soma. These spines have been identified as the direct targets of thalamocortical axons[23] and might, therefore, underlie the change in thalamocortical connection strength. The critical period profile can be manipulated by acting on this process directly. Here, we provide evidence of accelerated morphological and functional plasticity in the absence of *Icam5*. Our results are consistent with spine pruning and re-growth characteristic of other critical periods, such as in the visual cortex[28]. Conversely, in the latter system, GABA circuits have been implicated in the onset, and various structural "brakes" such as peri-neuronal nets or myelin-related signaling, in the closure of plasticity[29]. It will be interesting to determine to what extent these mechanisms also apply in A1.

Consistent with observations made for brainstem tonotopy[30], thalamocortical topography was already organized at hearing onset (Fig.3). Therefore, topographic organization is established prior to sensory experience. By VSDI of sub-threshold input, topography *in vitro* is well correlated to tonotopy *in vivo*[13]. As shown here, both are modified during a brief critical period from P12–P15 in mice exposed to abnormal acoustic environments. Behaviorally in rats, such plasticity is known to impair the perception of the over-represented frequency, while improving the discrimination of immediately adjacent frequencies[31].

The critical period for topographic plasticity defined here can be predicted by examining the day-by-day development of connectivity in normally-reared animals. During this maturation process, the direct cortical targets of thalamic input shift from deeper regions to L4 (Fig.5), where the number of stubby spines nearest the soma increases significantly. The temporal overlap of these changes in L4 may largely contribute to the *in vivo* tonotopic map reorganization following passive tone exposure (Fig.1) given the lack of tonotopic map

changes in the MGBv (Fig.2). However, this does not preclude additional changes at other intracortical sites during the critical period, such as potential refinement of local excitatory-inhibitory balance[32,33]. Detailed analysis of the developing cortical microcircuit, as already described for the mature auditory cortex[34], will be informative.

Isolating a developmental plasticity at the thalamocortical connection neither precludes potential changes in other sub-cortical regions reflecting auditory experience. Indeed, auditory plasticity has been reported in the midbrain and brainstem circuits, but has typically been associated with sensorineural hearing loss[30,35] or prolonged stimulus manipulations[36–39]. It has yet to be demonstrated whether sub-cortical reorganization occurs there *de novo* or is brought about by changes first arising in A1 that are then reflected in midbrain or brainstem nuclei via corticofugal inputs[40,41]. The auditory cortex itself is known to exhibit sequential critical periods beyond tonotopy[6,42,43]. For example, following the closure of a critical period for tonotopic map reorganization, we continued to observe rearing-induced changes in tuning bandwidth. Notably, the latter changes were observed not only in A1, but also in the MGBv (Supplementary Fig.1). Thus, it will be important to understand how subsequent stages of plasticity are related to the initial refinement of thalamocortical connections.

Supplementary Material

Refer to Web version on PubMed Central for supplementary material.

ACKNOWLEDGMENTS

References

1. Hensch TK. Critical period regulation. Annu Rev Neurosci. 2004; 27:549–579. [PubMed: 15217343]

2. Keuroghlian AS, Knudsen EI. Adaptive auditory plasticity in developing and adult animals. Prog Neurobiol. 2007; 82:109–121. [PubMed: 17493738]

3. Werker JF, Tees RC. Speech perception as a window for understanding plasticity and commitment in language systems of the brain. Dev Psychobiol. 2005; 46:233–251. [PubMed: 15772961]

4. Sanes DH, Bao S. Tuning up the developing auditory CNS. Curr Opin Neurobiol. 2009; 19:188–199. [PubMed: 19535241]

5. de Villers-Sidani E, Chang EF, Bao S, Merzenich MM. Critical period window for spectral tuning defined in the primary auditory cortex (A1) in the rat. J Neurosci. 2007; 27:180–189. [PubMed: 17202485]

6. Insanally MN, Kover H, Kim H, Bao S. Feature-dependent sensitive periods in the development of complex sound representation. J Neurosci. 2009; 29:5456–5462. [PubMed: 19403813]

7. King AJ, Nelken I. Unraveling the principles of auditory cortical processing: can we learn from the visual system? Nat Neurosci. 2009; 12:698–701. [PubMed: 19471268]

8. Wiesel TN, Hubel DH. Comparison of the effects of unilateral and bilateral eye closure on cortical unit responses in kittens. J Neurophysiol. 1965; 28:1029–1040. [PubMed: 5883730]

9. Hensch TK. Critical period plasticity in local cortical circuits. Nat Rev Neurosci. 2005; 6:877–888. [PubMed: 16261181]

10. Winer JA, Miller LM, Lee CC, Schreiner CE. Auditory thalamo-cortical transformation: structure and function. Trends Neurosci. 2005; 28:255–263. [PubMed: 15866200]

11. Cruikshank SJ, Rose HJ, Metherate R. Auditory thalamocortical synaptic transmission in vitro. J Neurophysiol. 2002; 87:361–384. [PubMed: 11784756]

12. Zhang LI, Bao S, Merzenich MM. Disruption of primary auditory cortex by synchronous auditory inputs during a critical period. Proc Natl Acad Sci USA. 2002; 99:2309–2314. [PubMed: 11842227]

13. Hackett TA, Rinaldi Barkat T, O'Brien BJ, Hensch TK, Polley DB. Linking topography to tonotopy in mouse auditory cortex. J Neurosci. 2011; 31:2983–2995. [PubMed: 21414920]

14. Winer JA, Sally SL, Larue DT, Kelly JB. Origins of medial geniculate body projections to physiologically defined zones of rat primary auditory cortex. Hear Res. 1999; 130:42–61. [PubMed: 10320098]

15. Kaur S, Rose HJ, Lazar R, Liang K, Metherate R. Spectral integration in primary auditory cortex: laminar processing of afferent input, in vivo and in vitro. Neuroscience. 2005; 134:1033–1045. [PubMed: 15979241]

16. Alford BR, Ruben RJ. Physiological, behavioral and anatomical correlates of the development of hearing in the mouse. Ann Otol Rhinol Laryngol. 1963; 72:237–247. [PubMed: 14012000]

17. Allendoerfer KL, Shatz CJ. The subplate, a transient neocortical structure: its role in the development of connections between thalamus and cortex. Annu Rev Neurosci. 1994; 17:185–218. [PubMed: 8210173]

18. Kanold PO, Luhmann HJ. The subplate and early cortical circuits. Annu. Rev. Neurosci. 2010; 33:23–48. [PubMed: 20201645]

19. Zhao C, Kao JPY, Kanold PO. Functional excitatory microcircuits in neonatal cortex connect thalamus and layer 4. J Neurosci. 2009; 29:15479–15488. [PubMed: 20007472]

20. Nakamura K, et al. Enhancement of hippocampal LTP, reference memory and sensorimotor gating in mutant mice lacking a telencephalon-specific cell adhesion molecule. Eur J Neurosci. 2001; 13:179–189. [PubMed: 11135016]

21. Matsuno H, et al. Telencephalin slows spine maturation. J Neurosci. 2006; 26:1776–1786. [PubMed: 16467526]

22. de Villers-Sidani E, et al. Manipulating critical period closure across different sectors of the primary auditory cortex. Nat Neurosci. 2008; 11:957–965. [PubMed: 18604205]

23. Richardson RJ, Blundon JA, Bayazitov IT, Zakharenko SS. Connectivity patterns revealed by mapping of active inputs on dendrites of thalamo-recipient neurons in the auditory cortex. J Neurosci. 2009; 29:6406–6417. [PubMed: 19458212]

24. Simons DJ. Response properties of vibrissa units in rat SI somatosensory neocortex. J Neurophysiol. 1978; 41:798–820. [PubMed: 660231]

25. Masino SA, Kwon MC, Dory Y, Frostig RD. Characterization of functional organization within rat barrel cortex using intrinsic signal optical imaging through a thinned skull. Proc Natl Acad Sci U S A. 1993; 90:9998–10002. [PubMed: 8234348]

26. Kleinfeld D, Delaney KR. Distributed representation of vibrissa movement in the upper layers of somatosensory cortex revealed with voltage-sensitive dyes. J Comp Neurol. 1996; 375:89–108. [PubMed: 8913895]

27. Petersen CC, Grinvald A, Sakmann B. Spatiotemporal dynamics of sensory responses in layer 2/3 of rat barrel cortex measured in vivo by voltage-sensitive dye imaging combined with whole-cell voltage recordings and neuron reconstructions. J Neurosci. 2003; 23:1298–1309. [PubMed: 12598618]

28. Mataga N, Mizuguchi Y, Hensch TK. Experience-dependent pruning of dendritic spines in visual cortex by tissue plasminogen activator. Neuron. 2004; 44:1031–1041. [PubMed: 15603745]

29. Morishita H, Hensch TK. Critical period revisited: impact on vision. Curr Op Neurobiol. 2008; 18:101–107. [PubMed: 18534841]

30. Kandler K, Clause A, Noh J. Tonotopic reorganization of developing auditory brainstem circuits. Nat Neurosci. 2009; 12:711–717. [PubMed: 19471270]

31. Han YK, Köver H, Insanally MN, Semerdjian JH, Bao S. Early experience impairs perceptual discrimination. Nat Neurosci. 2007; 10:1191–1197. [PubMed: 17660815]

32. Dorrn AL, Yavan K, Barker AJ, Schreiner CE, Froemke RC. Developmental sensory experience balances cortical excitation and inhibition. Nature. 2010; 465:932–936. [PubMed: 20559387]

33. Sun YJ, et al. Fine-tuning of pre-balanced excitation and inhibition during auditory cortical development. Nature. 2010; 465:927–931. [PubMed: 20559386]

34. Oviedo HV, Bureau I, Svoboda K, Zador AM. The functional asymmetry of auditory cortex is reflected in the organization of local cortical circuits. Nat Neurosci. 2009; 13:1413–1420. [PubMed: 20953193]

35. Harris JA, Rubel EW. Afferent regulation of neuron number in the cochlear nucleus: cellular and molecular analyses of a critical period. Hear Res. 2006; 216:127–137. [PubMed: 16874907]

36. Smith ZD, Gray L, Rubel EW. Afferent influences on brainstem auditory nuclei of the chicken: n. laminaris dendritic length following monaural conductive hearing loss. J Comp Neurol. 1983; 220:199–205. [PubMed: 6315783]

37. Seidl AH, Grothe B. Development of sound localization mechanisms in the mongolian gerbil is shaped by early acoustic experience. J Neurophysiol. 2005; 94:1028–1036. [PubMed: 15829592]

38. Sanes DH, Constantine-Paton M. Altered activity patterns during development reduce neural tuning. Science. 1983; 16:1183–1185. [PubMed: 6612332]

39. Mogdans J, Knudsen EI. Site of auditory plasticity in the brain stem (VLVp) of the owl revealed by early monaural occlusion. J Neurophysiol. 1994; 72:2875–2891. [PubMed: 7897496]

40. Yan W, Suga N. Corticofugal modulation of the midbrain frequency map in the bat auditory system. Nat Neurosci. 1998; 1:54–58. [PubMed: 10195109]

41. Bajo VM, Nodal FR, Moore DR, King AJ. The descending corticocollicular pathway mediates learning-induced auditory plasticity. Nat Neurosci. 2010; 13:253–260. [PubMed: 20037578]

42. Popescu MV, Polley DB. Monaural deprivation disrupts development of binaural selectivity in auditory midbrain and cortex. Neuron. 2010; 65:718–731. [PubMed: 20223206]

43. Razak KA, Richardson MD, Fuzessery ZM. Experience is required for the maintenance and refinement of FM sweep selectivity in the developing auditory cortex. Proc Natl Acad Sci U S A. 2008; 105:4465–4470. [PubMed: 18334643]

44. Stiebler I, Neulist R, Fichtel I, Ehret G. The auditory cortex of the house mouse: left-right differences, tonotopic organization and quantitative analysis of frequency representation. J Comp Physiol A. 1997; 181(6):559–571. [PubMed: 9449817]

45. Grinvald A, Hildesheim R. VSDI: a new era in functional imaging of cortical dynamics. Nat Rev Neurosci. 2004; 5:874–885. [PubMed: 15496865]

46. Ferezou I, Bolea S, Petersen CCH. Visualizing the cortical representation of whisker touch: voltage-sensitive dye imaging in freely moving mice. Neuron. 2006; 50:617–629. [PubMed: 16701211]

47. Zhou X, Nagarajan N, Mossop BJ, Merzenich MM. Influences of un-modulated acoustic inputs on functional maturation and critical-period plasticity of the primary auditory cortex. Neuroscience. 2008; 154(1):390–396. [PubMed: 18304741]

48. Kim H, Bao S. Selective increase in representations of sounds repeated at an ethological rate. J Neurosci. 2009; 29(16):5163–5169. [PubMed: 19386912]

49. Geissler DB, Ehret G. Auditory perception vs. recognition: representation of complex communication sounds in the mouse auditory cortical fields. Eur J Neurosci. 2004; 19(4):1027–1040. [PubMed: 15009150]

50. Gan WB, Grutzendler J, Wong WT, Wong RO, Lichtman JW. Multicolor "DiOlistic" labeling of the nervous system using lipophilic dye combinations. Neuron. 2000; 27:219–225. [PubMed: 10985343]
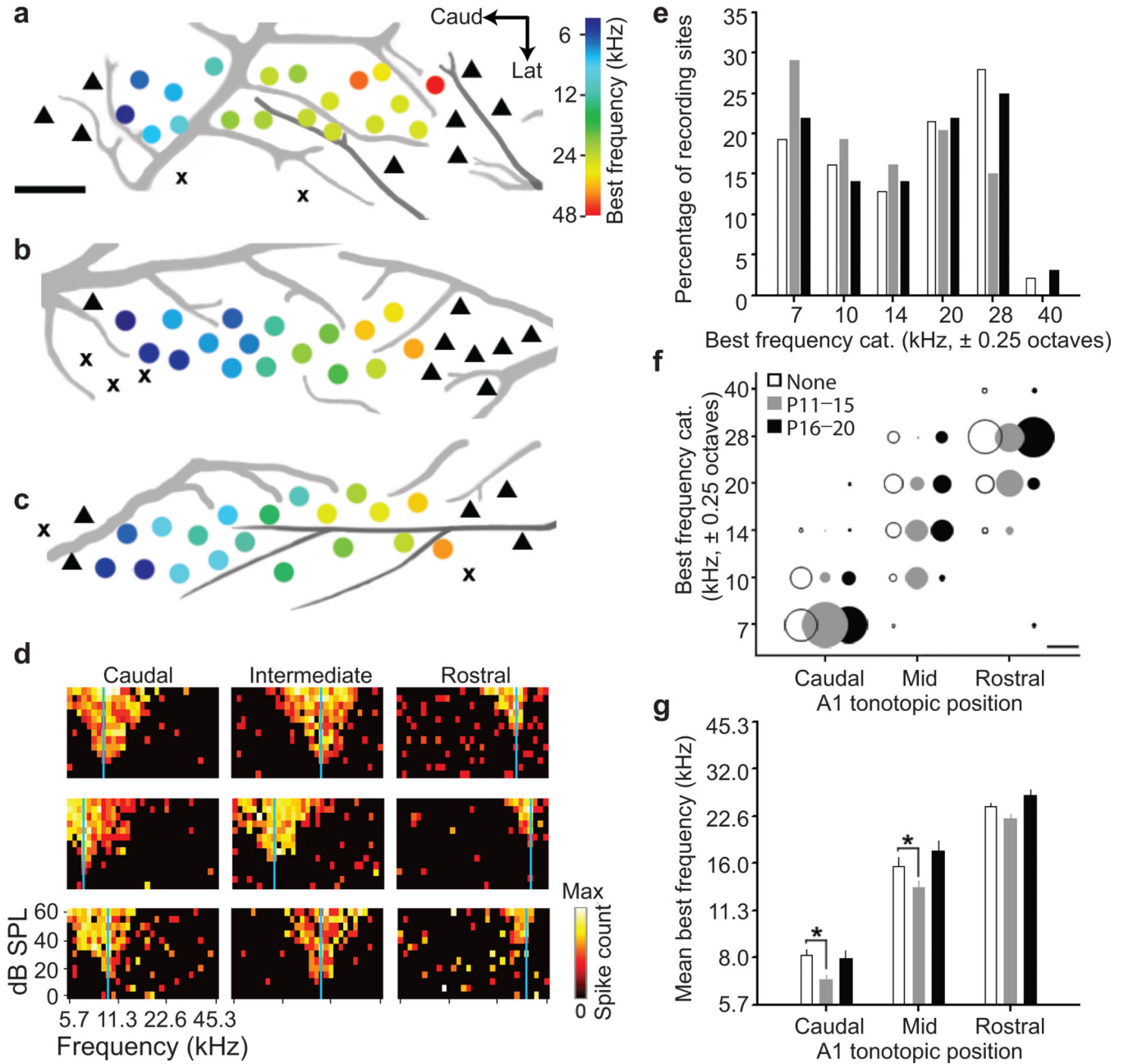
Author Manuscript

Author Manuscript

Author Manuscript

Author Manuscript

Figure 1. Developmental cortical map reorganization in mouse A1

Representative A1 best frequency maps from the left hemisphere of young adult mice (P32–39) reared in a normal sound environment (**a**) or after 7 kHz tone exposure between P11–P15 (**b**) or P16–20 (**c**). Circle denotes multi-unit recording site and hue represents best frequency (color scale). triangle = non-A1 recording site, x = non-responsive site. Scale bar, 0.25 mm. Black and grey lines represent branches of the middle cerebral artery and inferior branches of the rhinal vein, respectively. **d**, Sample frequency response areas of normalized firing rates as a function of tone frequency and level. Recordings obtained from caudal, intermediate and rostral zones of A1 from mice reared in a normal sound environment (top row), or with 7 kHz tones between P11–P15 (middle row) or P16–P20 (bottom row).

Vertical blue line indicates best frequency. **e**, Percentage of recording sites of all best frequency measurements in normally reared mouse A1 (open bars; n=18,15,12,20,26,2 sites for each of the six categories) or those reared with 7 kHz tones between P11–P15 (grey bars; n=27,18,15,19,14,0 sites) or P16–P20 (black bars, n=14,9,9,14,16,2 sites). Best frequencies are grouped into 0.5 octave bins centered on the X-axis frequency. **f**, Best frequency distributions segregated by rearing condition and topographic location. Percentage of best frequency sites is represented by circle diameter. Scale bar denotes a diameter equalling 50% of the distribution. **g**, Best frequency values (mean ± s.e.m.) for each rearing group and topographic position. * $P < 0.05$ (t-test).
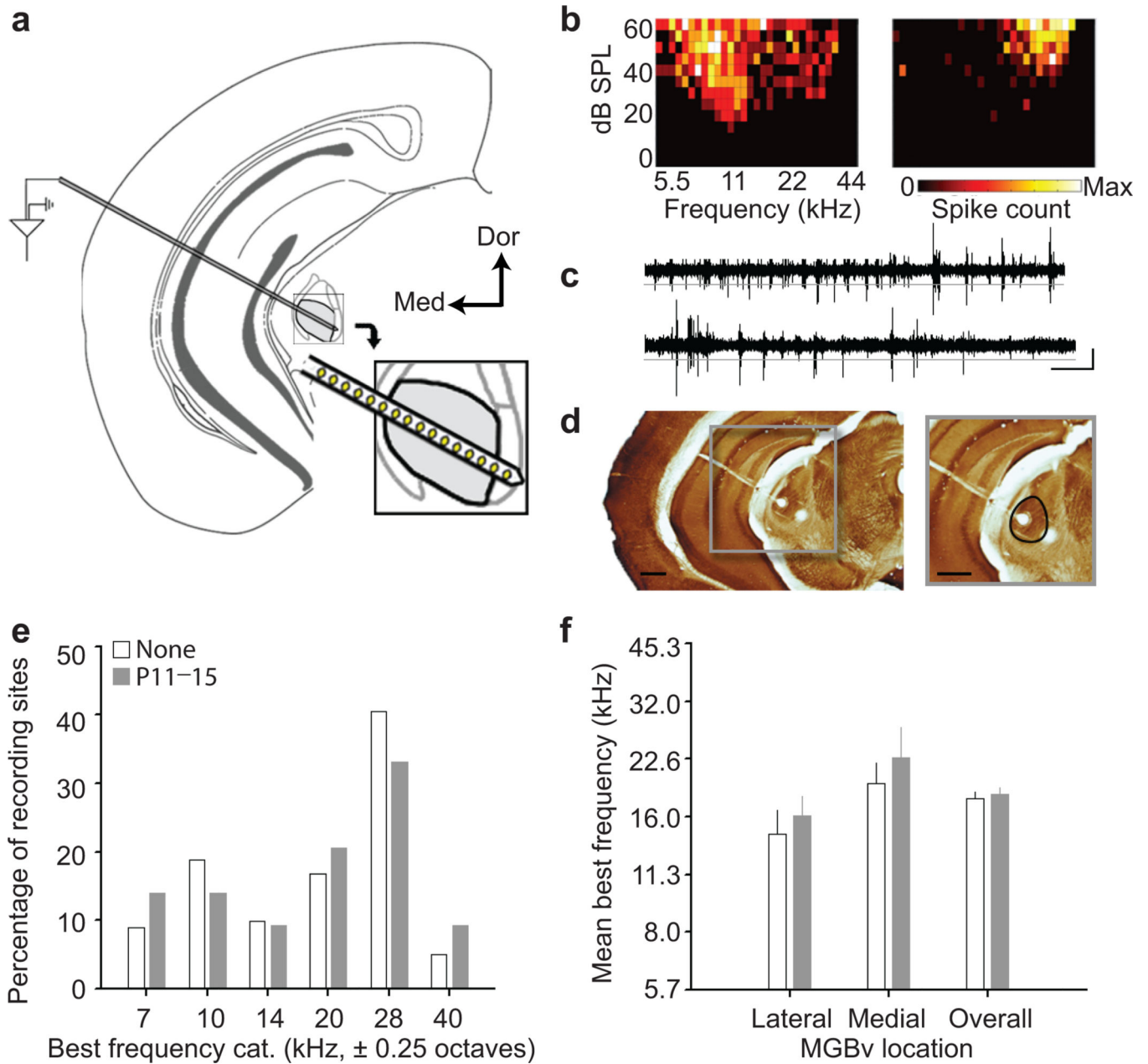
Figure 2. Thalamic tonotopy remains stable despite reorganization of A1 maps
a, *In vivo* recordings from MGBv (grey shading) by a multichannel silicon probe inserted at an angle matching the plane of thalamocortical slices. Inset, schematic depicting position of recording sites relative to cytoarchitectonic boundaries of MGBv. **b**, Sample frequency response areas recorded from a lateral (left) and medial (right) recording site. All conventions match those in Fig.1d. **c**, Examples of raw multiunit traces recorded with a tungsten microelectrode used for A1 mapping (upper) or silicon probe used for MGBv mapping (lower). Spikes were registered when signal amplitude exceeded a threshold line set at 4 s.d. from the mean of a 5 sec running average (indicated by grey line). Scale bar, 1 sec, 0.1 mV. **d**, Images of coronal section through MGBv reacted for cytochrome oxidase.

High-power image depicts the location of two lesions made within and outside the MGBv boundary (black outline). Scale bar, 0.5 mm. **e**, Percentage of recording sites of all best frequency measurements from normally reared mouse MGBv (open bars; n=9,19,10,17,41,5 sites for each of the six categories) and those reared with 7 kHz tones between P11–P15 (grey bars; n=21,21,14,31,50,14 sites). **f**, Best frequency values (mean ± s.e.m.) measured at lateral (0.05 mm past the lateral MGBv boundary) or medial loci (0.2 mm past the lateral MGBv boundary), as well as averaged overall.
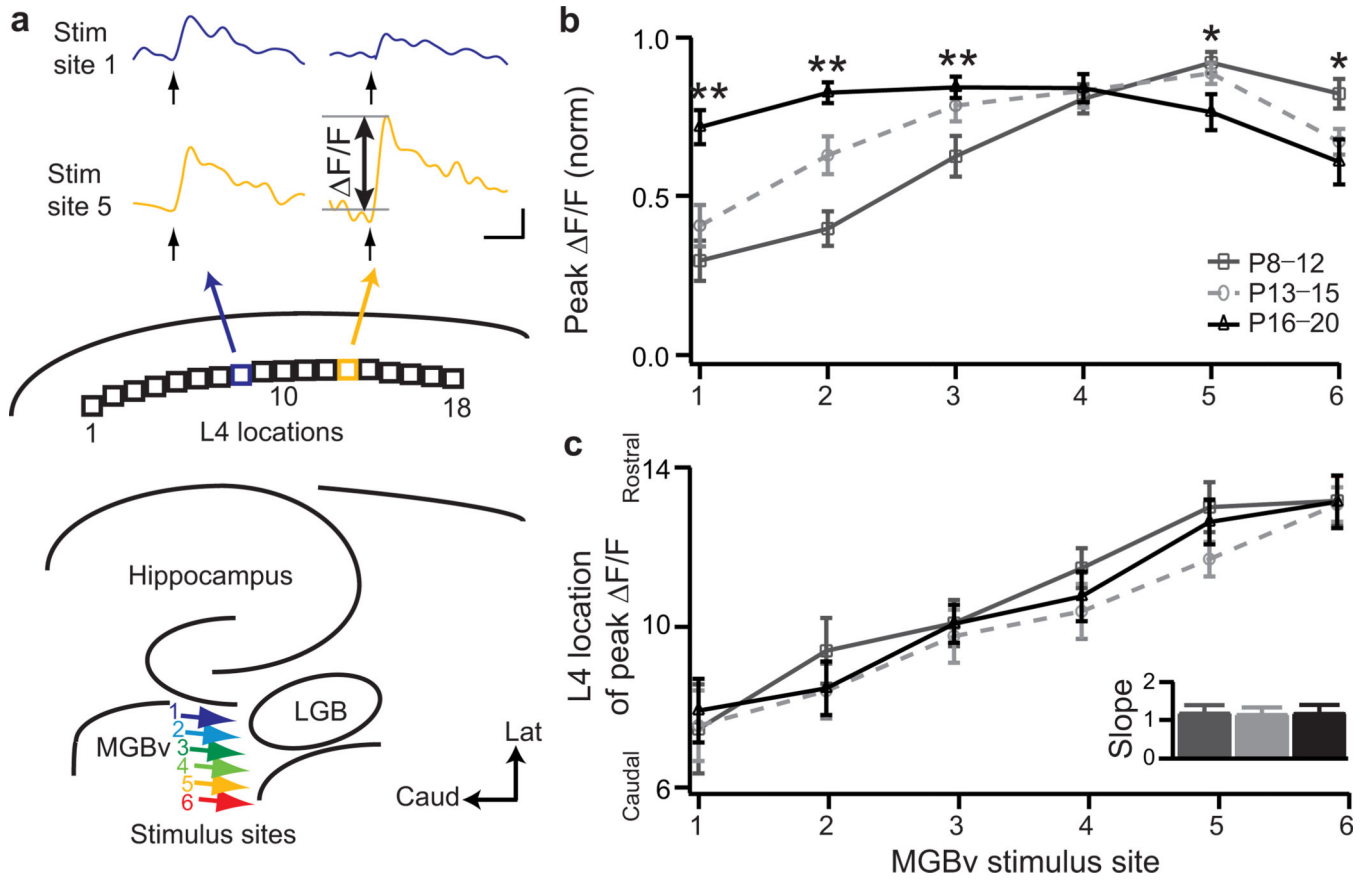
Figure 3. Topography and developmental window for A1 response strengthening at P12–P15
a, Schematic of the six MGBv stimulus sites (colored arrows) and eighteen L4 locations analyzed in A1. Sample traces of ΔF/F at two different L4 loci (8 and 13) as a function of time following a 1 ms stimulus pulse to MGBv site 1 (blue) or 5 (yellow). P12 control mouse. Scale bar, 100 ms, 0.1% ΔF/F. **b**, Normalized peak ΔF/F as a function of stimulus site for 3 age groups (mean ± s.e.m.; P8–P12, n=13; P13–P15, n=16; P16–P20, n=16). * $P<0.05$; ** $P<0.01$ (t-test) between dark grey and black. **c**, Peak ΔF/F location in L4 as a function of MGBv stimulus site. Inset, topographic slope (mean ± s.e.m.) for the 3 age groups.
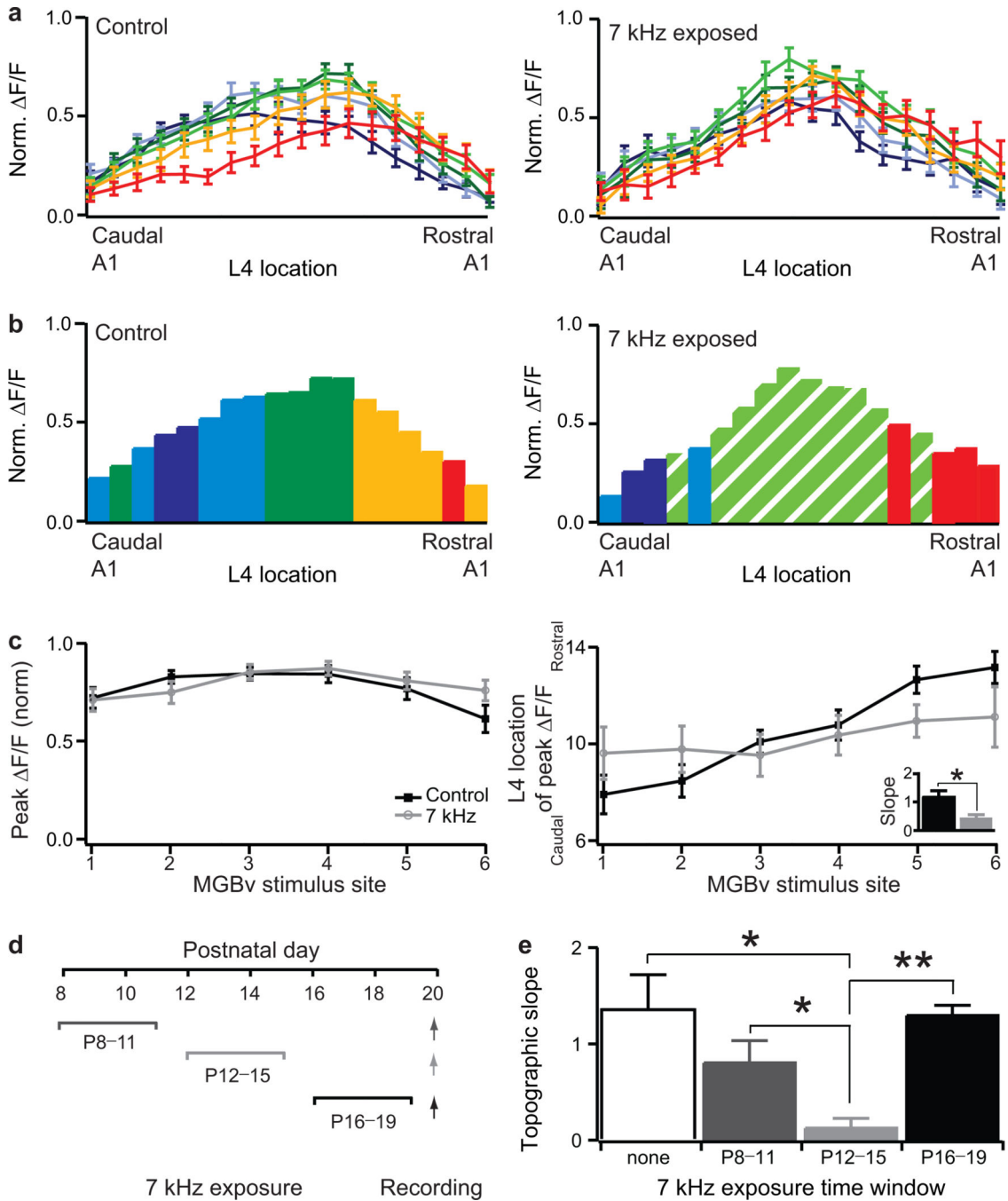
Figure 4. Critical period for experience-dependent topographic refinement at P12–P15
a and **b**, Normalized maximal F/F across L4 loci in response to different MGBv stimulus
sites for P16–P20 mice raised in a normal acoustic environment (left panel, n=16) or
exposed to a 7 kHz tone from P8 (right panel, n=13). Color code indicates MGBv stimulus
site as in Fig.3a. **c**, Normalized peak F/F, defined as maximum F/F amplitude across all
L4 loci, and location of L4 peak F/F in response to different MGBv stimulus site for P16–
P20 control and 7 kHz exposed mice. Inset, topographic slopes. (mean ± s.e.m.) * $P<0.05$ (t-
test). **d**, Schedule of tone exposure windows and recording (arrows). **e**, Topographic slopes

(median ± s.e.m.) for control mice (none, n=9) and those exposed to 7 kHz during three time windows (P8–P11, n=8; P12–P15, n=8; P16–P19, n=5). ** P<0.01 (Mann-Whitney U test).
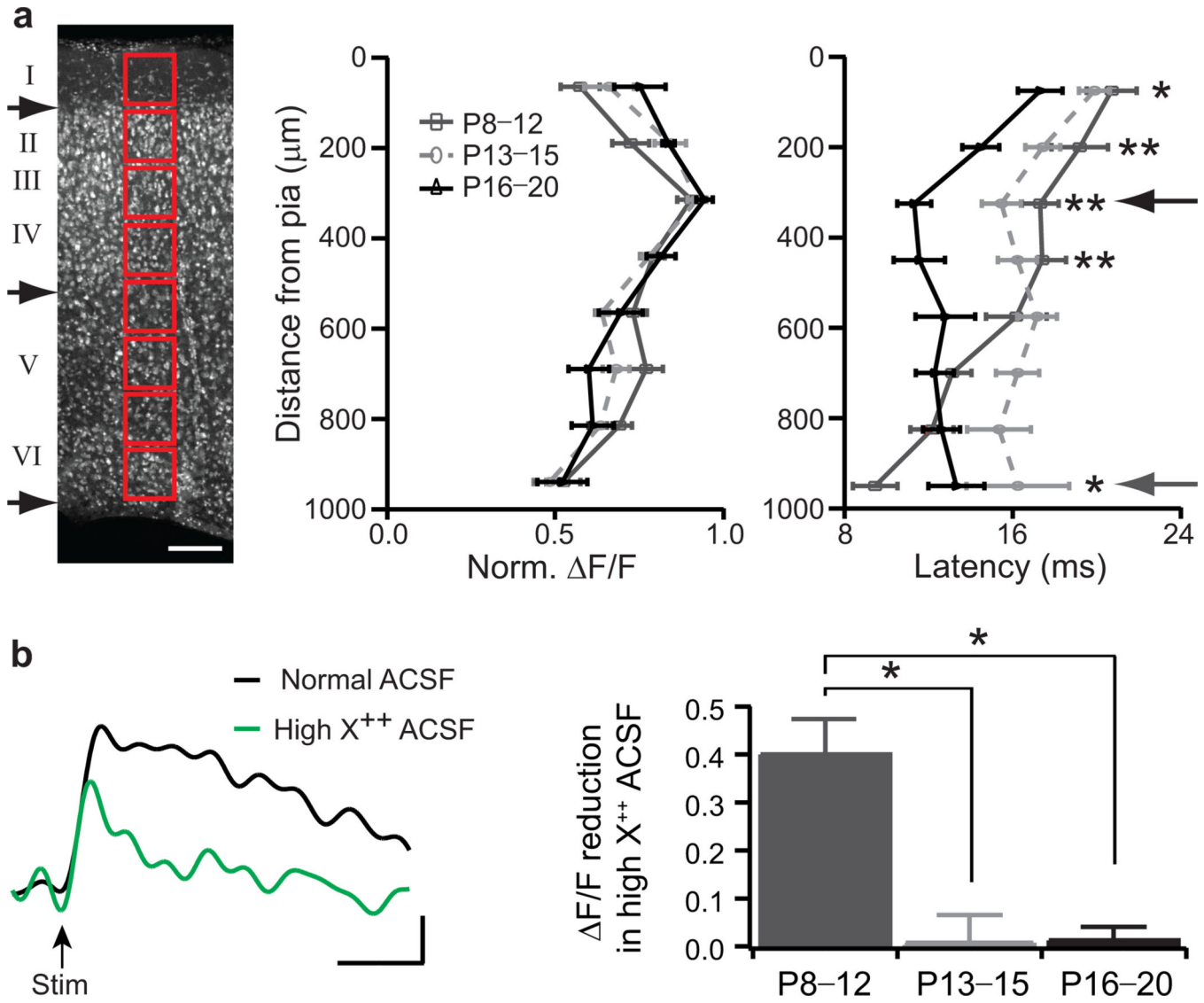
Figure 5. Columnar shift of thalamocortical connectivity up to L4 through the critical period
a, Nissl stain of a P20 thalamocortical slice for columnar analysis (red boxes). Black arrows denote approximate borders between layers I/II, layers IV/V and layer VI/white matter. Scale bar, 125 μm. Normalized ΔF/F and latency with distance from pia for 3 age groups (mean ± s.e.m.; P8–P12, n=13; P13–P15, n=15; P16–P20, n=11). * $P<0.05$; ** $P<0.01$ (t-test) between dark grey and black. **b**, Sample upper L4 cortical response at P10 in normal (black) and high X^{++} (green) ACSF. Scale bar, 100 ms, 0.2% ΔF/F. Response reduction (median ± s.e.m.) in high X^{++} for 3 age groups (P8–P12, n=6; P13–P15, n=8; P16–P20, n=4). * $P<0.05$ (Mann-Whitney U test).
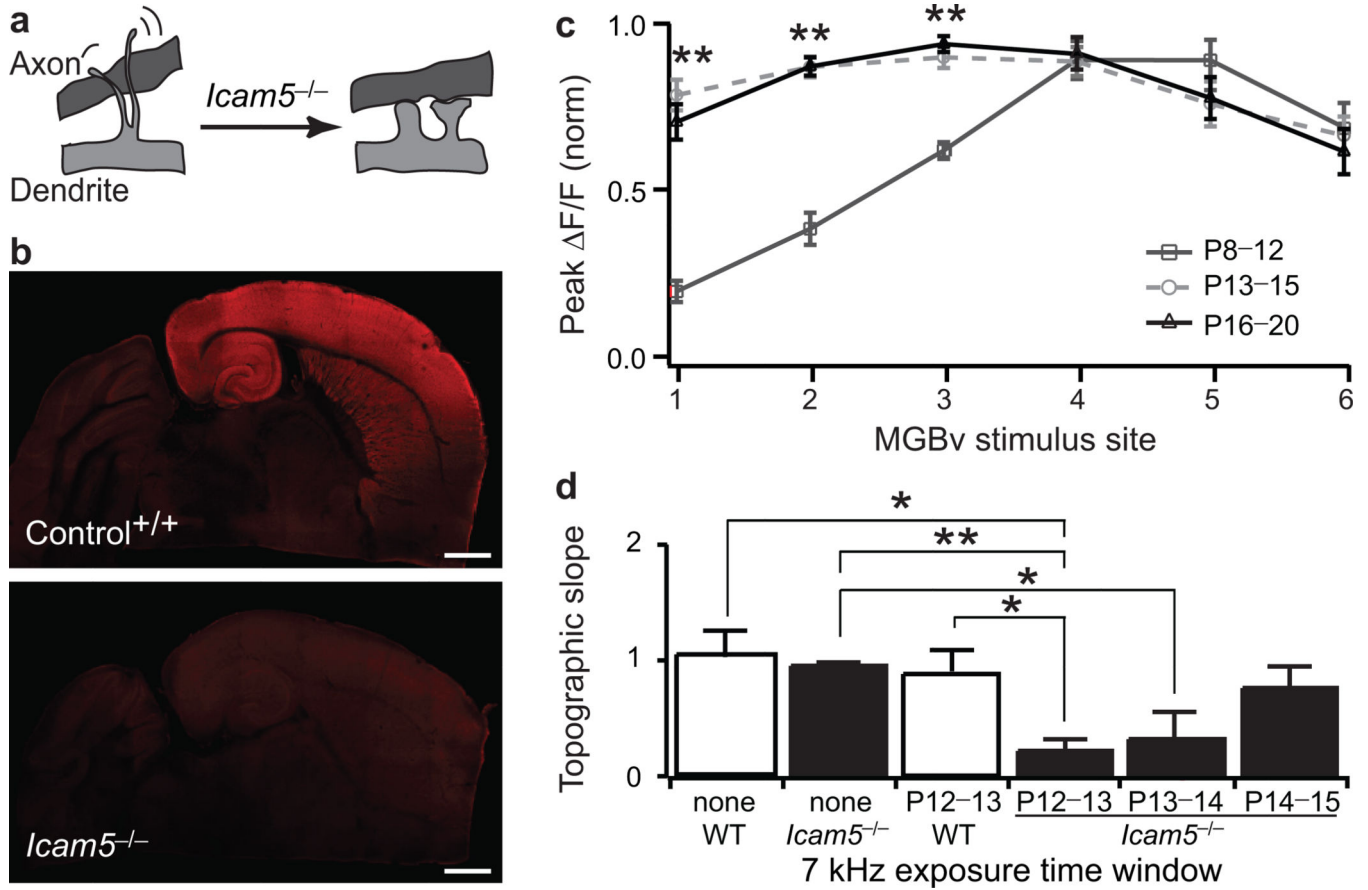
Figure 6. Forebrain-specific gene deletion accelerates thalamocortical plasticity
a, *Icam5* normally slows dendritic spine maturation[21]. **b**, *Icam5* expression at P13 in the auditory thalamocortical slice. Note absence of immunostaining in control MGBv and throughout *Icam5*−/− brain. Scale bar, 1mm. **c**, Normalized peak F/F as a function of MGBv stimulus site in *Icam5*−/− mice for three age groups (median ± s.e.m.; P8–P12, n=8; P13–P15, n=10; P16–P20, n=9). ** *P*<0.01 (Mann-Whitney U test) between dark grey and black. **d**, Topographic slope (median ± s.e.m.) for mice without (none, wild-type, n=15; *Icam5*−/−, n=9) or after 7 kHz exposure between P12–P13 (wild-type, n=9; *Icam5*−/−, n=7), P13–P14 (*Icam5*–/−, n=9) or P14–P15 (*Icam5*–/−, n=9). * *P*<0.05, ** *P*<0.01 (Mann-Whitney U test).
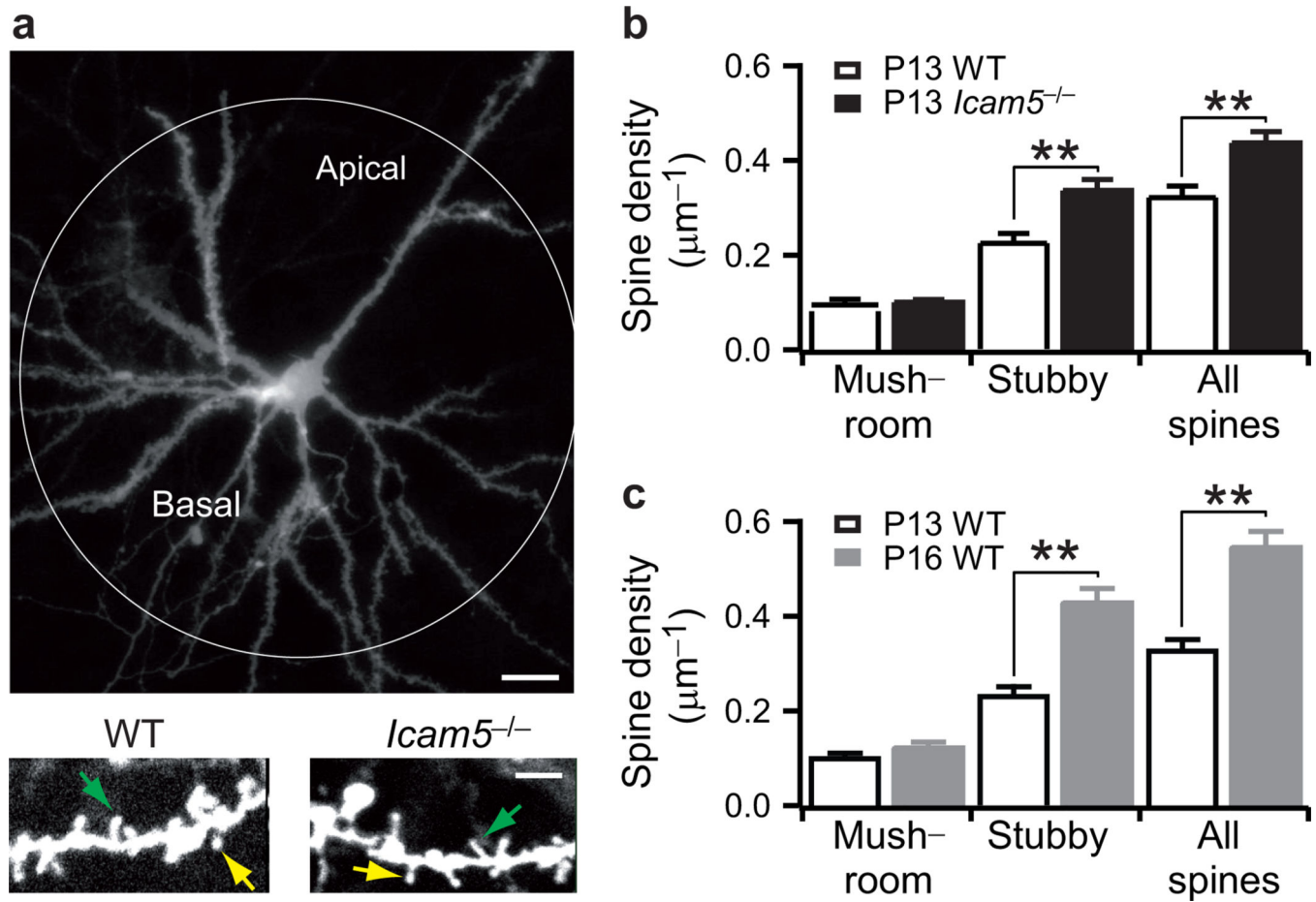
Figure 7. Stubby spine density increases through the critical period
a, Sample DiI-labeled upper L4 pyramidal cell. Scale bar, 20 μm (upper panel). High-power image of dendrites at P13 revealing mushroom (yellow arrow) and stubby spines (green arrow). Scale bar, 5 μm (lower panel). **b**, Spine density in P13 wild-type (n=6) and *Icam5*$^{-/-}$ mice (n=7 neurons). **c**, Spine density (median±s.e.m.) in P13 (n=6) and P16 wild-type mice (n=7 neurons). ** *P*<0.01 (Mann-Whitney U test).